ACS central science

Research Article

Cite This: ACS Cent. Sci. 2018, 4, 590−599

On-Chip in Situ Monitoring of Competitive Interfacial Anionic Chemisorption as a Descriptor for Oxygen Reduction Kinetics

Mengning Ding,[†,§,#] Guangyan Zhong,[‡] Zipeng Zhao,[†] Zhihong Huang,[†] Mufan Li,[‡] Hui-Ying Shiu,[†] Yuan Liu,[†,§] Imran Shakir,[∥] Yu Huang,*[,†,§] and Xiangfeng Duan*[,‡,§]

[†]Department of Materials Science and Engineering, [‡]Department of Chemistry and Biochemistry, and [§]California Nanosystems Institute, University of California, Los Angeles, California 90095, United States

[∥]Sustainable Energy Technologies Centre, College of Engineering, King Saud University, Riyadh 11421, Kingdom of Saudi Arabia

Supporting Information

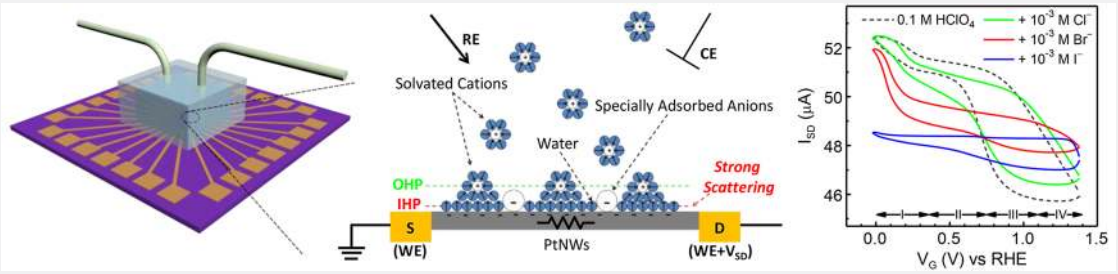

ABSTRACT: The development of future sustainable energy technologies relies critically on our understanding of electrocatalytic reactions occurring at the electrode−electrolyte interfaces, and the identification of key reaction promoters and inhibitors. Here we present a systematic in situ nanoelectronic measurement of anionic surface adsorptions (sulfates, halides, and cyanides) on ultrathin platinum nanowires during active electrochemical processes, probing their competitive adsorption behavior with oxygenated species and correlating them to the electrokinetics of the oxygen reduction reaction (ORR). The competitive anionic adsorption features obtained from our studies provide fundamental insight into the surface poisoning of Pt-catalyzed ORR kinetics by various anionic species. Particularly, the unique nanoelectronic approach enables highly sensitive characterization of anionic adsorption and opens an efficient pathway to address the practical poisoning issue (at trace level contaminations) from a fundamental perspective. Through the identified nanoelectronic indicators, we further demonstrate that rationally designed competitive anionic adsorption may provide improved poisoning resistance, leading to performance (activity and lifetime) enhancement of energy conversion devices.

INTRODUCTION

Electrocatalysis plays a central role in sustainable energy-conversion/storage technologies.[1−5] For instance, platinum and other transition metal catalyzed oxygen reduction reaction (ORR) is critical for fuel cells, batteries, and other electro-/photocatalytic processes.[6,7] The intrinsic ORR activities have been significantly improved over the past decade by using specifically designed electrocatalysts (size, shape, composition, morphology, and electronic structure of the nanostructures).[8−13] However, such extraordinary performance of new catalyst materials is usually only achieved in laboratory model studies (e.g., rotating disk electrode measurements) under a highly controlled environment. There has been considerable challenge in delivering their promise in practical energy devices with a less controlled environment, partly due to the complex interfacial adsorption that could severely degrade the electrochemical performance.[14] Therefore, fundamental understanding of the electrochemical interface (encompassing catalyst surface and electrolyte double layer structure), where key physical interactions and chemical transformations (adsorption, bonding reformation, desorption, etc.) occur, is vital for optimizing electrochemical reactions in less controlled, complex chemical environments. To this end, in situ or in operando characterizations that can reveal chemical details at such an interface during the active reaction cycles is essential for establishing a fundamental basis and guiding the rational design of highly active and long-lasting catalysts, yet they are insufficiently explored due to extreme technical challenges.

The classic picture of an electrochemical interface involves molecules, intermediates, solid electrode surface, and the surrounding electrolyte double layer. Such complexity often interferes with any form of radiation signals from a specific target (e.g., FTIR signals from surface adsorbed chemical species), posing considerable technical difficulties in the implement of conventional spectroscopic strategies for in situ electrochemical characterizations. Alternatively, there has been an increasing interest in the development of integrated and comprehensive on-chip characterization approaches, which in certain cases offer specific advantages, as additional new tools

Received: February 4, 2018
Published: April 25, 2018

DOI: 10.1021/acscentsci.8b00082
ACS Cent. Sci. 2018, 4, 590−599

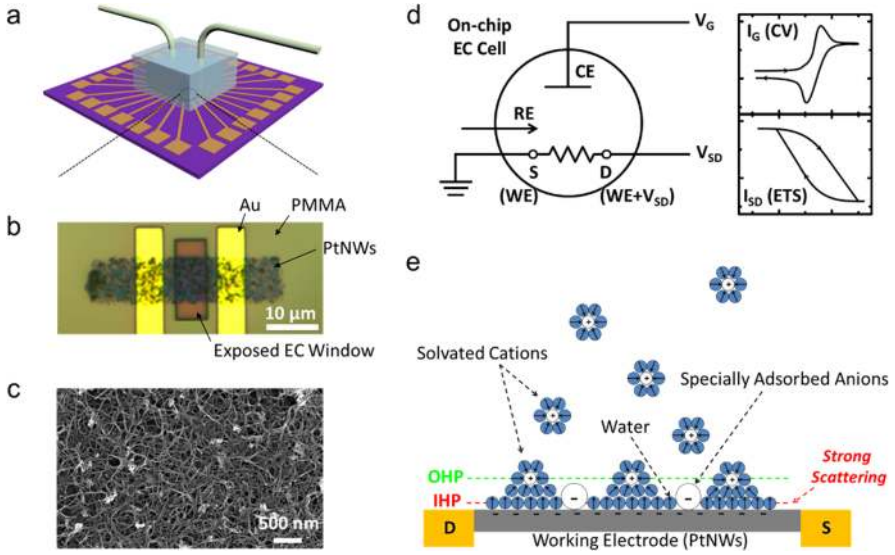

Figure 1. Schematic illustration of experimental setup and working principle of the on-chip cyclic voltammetry (CV) and electrical transport spectroscopy (ETS) measurement. (a) Schematic illustration of the microfluidic system for the on-chip electrochemical and nanoelectronic measurements. (b) Optical microscopic image (OM) of an on-chip cell (enlarged area in a) showing PMMA (electrochemically inert) covered gold electrodes, and the exposed PtNWs network in the opened PMMA window. (c) SEM image of the PtNWs network. (d) Schematic diagram for the working principles of concurrent CV and ETS. CE, counter electrode; RE, reference electrode; WE, working electrode; S, source; D, drain. (e) Schematic illustration of the double layer model for PtNW electrode in an aqueous electrolyte with specific adsorption of anions at the inner Helmholtz plane (IHP).

for the mechanistic study of key electrochemical process in the material research.[15−19] Specifically, exploiting the chemical sensitivity of nanomaterials that can be transformed into electrical signals, we have recently developed electrical transport spectroscopy (ETS) that offers a complementary on-chip signaling technique for in situ studies of electrochemical interfaces.[15] By conducting concurrent electrochemical and nanoelectronic measurements of metallic nanocatalysts, the ETS measurements produce a signal that is highly sensitive to the dynamic surface states during active electrochemical processes based on surface scattering of the conduction electrons in metallic nanocatalysts. Such highly surface-specific signals can be correlated with the adsorption of electroactive reactant molecules and intermediate species on the catalyst surface, revealing the catalytic surface states in action and offering valuable new insights into the reaction mechanisms.

Here we present a systematic study of the anionic adsorption on a platinum nanowire surface. In a practical electrocatalytic device, anions may come from a functioning electrolyte, chemical source in other components, or undesired contaminations. The presence of these anions often results in competitive adsorption on the catalyst surface (located within the inner Helmholtz plane (IHP)), which could potentially block the adsorption of electroactive reactant molecules or hinder the formation of intermediate species, leading to a catalyst poisoning effect. As a result, anionic chemisorption is generally believed to affect the electrode kinetics in a wide range of reactions such as ORR, hydrogen evolution reaction (HER), and oxidation of organic molecules.[20] To this end, we show that ETS provides a direct "visualization" of distinct adsorption features, which allows detailed analysis of surface anionic adsorptions to derive quantitative information unravelling the rich complexity in such electrochemical interfaces. We present a competitive anionic adsorption model as a descriptor for the ORR activity and the poisoning effect on Pt surface, which is further supported by the standard rotating disk electrode (RDE) evaluations. On the basis of the correlation between Pt-catalyzed ORR activity and surface anionic adsorption/competitions, we attribute the existing performance gap of ORR catalysts between laboratory model studies and practical energy devices to the anionic contaminations under practical conditions. More importantly, we further investigate the competitive adsorption of mixed anions, which suggests potential strategies for designing more poisoning-resistant catalytic systems to mitigate the undesired anionic chemisorption poisoning.

EXPERIMENTAL APPARATUS

Figure 1a depicts the schematic experimental set up of concurrent electrochemical and ETS studies, while more experimental details can be found in Methods and Supplementary Figure S1. Ultrafine platinum nanowires (PtNWs) prepared through wet chemistry[21] were chosen as the model catalytic material. Briefly, nanoelectronic devices were fabricated by selectively depositing a thin film of PtNWs onto the Si/SiO_2 substrate with prepatterned gold electrodes. An electrochemically inert layer (PMMA) was then coated on top of the device with an electrochemical window defined by electron-beam lithography. The morphology of the PtNW network was examined by optical microscopy (OM, Figure 1b and Supplementary Figure S1) and scanning electron microscopy (SEM, Figure 1c). A microfluidic setup was used for highly efficient control of the electrolytes exposed to the PtNW device. A leak-free reference electrode (RE, Harvard Apparatus LF-2) was employed to eliminate the potential influence of electrolyte leakage (most importantly anions) from the RE to the testing environment. The working principle of ETS is shown in Figure 1c. A two-channel source-measure-unit (SMU, Agilent 2902a) was employed for ETS measurements, one for applying gate voltage (V_G) and collecting the gate Faradaic current (I_G, corresponding to the electrochemical

DOI: 10.1021/acscentsci.8b00082
ACS Cent. Sci. 2018, 4, 590−599

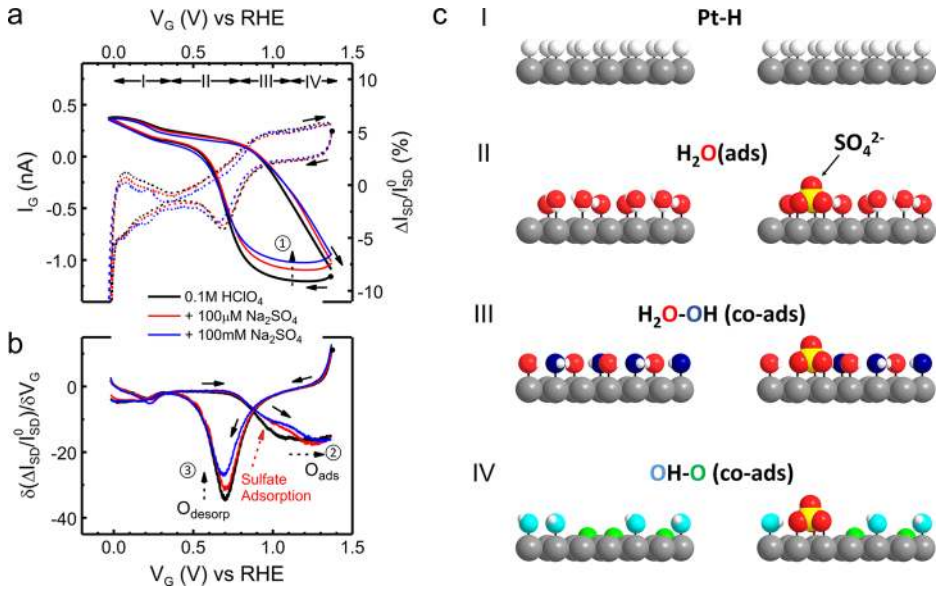

Figure 2. In situ electrical transport spectroscopy (ETS) of sulfate adsorption on Pt surface. (a) I_G-V_G (on-chip CV, dashed curves) and normalized $I_{SD}-V_G$ (ETS, solid curves) characteristics of a typical PtNW device in 0.1 M $HClO_4$ (black) and with addition of varying concentrations of sulfate anions (red and blue). The CV results resemble the typical CV characteristic of a polycrystalline Pt surface, containing redox regions of under potential hydrogen adsorption (region I); the double layer (region II), reversible adsorption of OH (region III), and surface oxide formation (region IV). (b) Differentiated analysis of ETS (dETS) results showing spectral peak characteristics. Dashed arrows (1 in a and 2, 3 in b) indicate the change of ETS or dETS results by the effect of sulfate adsorption. (c) Schematic models of different Pt surface conditions in different electrochemical regions in $HClO_4$ and with sulfate anions. Pt atoms are gray, H atoms are white, O atoms are red in H_2O_{ads}, blue in OH_{ads}, and green in O_{ads} for a visual guide to the different scattering effects. Solid arrows in all figures indicate the potential sweeping direction, with corresponding dots showing the starting point of the measurement.

current in a typical cyclic voltammetry (CV) measurement), and the other for in situ measurement of the electrical properties of PtNW device, i.e., ETS signals (see Methods and Supplementary Figure S2). In the classic double layer model (Figure 1d), the chemisorbed anions are located in the inner Helmholtz plane (IHP), which is buried between solid−liquid electrochemical interfaces. Such electrochemical interfaces are difficult to access by the radiation, but can be easily probed by electrical current in the ultrafine metallic nanostructures that is highly sensitive to the surface scattering effect of the adsorbed chemical species.

RESULTS AND DISCUSSION

Sulfate Adsorption on PtNWs. Surface adsorption of sulfate anions on the PtNWs was first investigated by acquiring their ETS characteristics in sulfate containing electrolyte solutions. As the chemical identity of the adsorbate, either in the form of HSO_4^-, SO_4^{2-}, or $SO_4^{2-}-H_3O^+$ complexes, has been under considerable debate, it is generally denoted here as sulfate.[20] For comparison, an ETS baseline with no sulfate adsorption was also established in 0.1 M perchloric acid, since the perchlorate ion has been considered as one of the weakest adsorbed anions on Pt and is used here as the background electrolyte for the investigation of other anion adsorptions. Figure 2a (black curve) shows typical CV[22] and ETS[15] baseline features of the PtNWs. First, the ETS current remains relatively flat in the double layer (D.L.) region (region II), where the PtNW surface is predominantly occupied by adsorbed water molecules. Second, in the more negative potential range, adsorption (desorption) of a monolayer of hydrogen atoms (H_{ads}) on the PtNW surface results in an obvious increase (decrease) in the ETS current (region I). The increase in conductance (G_{SD}) during the H adsorption can be attributed to a more predominant specular scattering of electrons (therefore less diffusive scattering) for a Pt−H surface than a Pt−H_2O surface.[15,23,24] Third, in the positive potential region, which corresponds to the adsorption/desorption of surface oxygenated species including reversible adsorption of hydroxyl groups (region III) and further oxidation that leads a surface oxide formation (region IV), a more pronounced G_{SD} signal (steep decrease in value due to larger scattering cross section of strongly bonded O species) is observed along with much larger hysteresis (due to the irreversible nature of oxide formation).

The surface adsorption of sulfate anions on polycrystalline Pt electrode have been previously studied with Fourier transform infrared (FTIR),[25,26] sum frequency generation (SFG),[27] or second harmonic generation (SHG)[28,29] spectroscopy in the double layer region at relatively higher concentrations (usually introduced as 0.5 M H_2SO_4). The use of high concentration sulfate ions was probably due to the relatively weak signals of surface sulfate under the testing conditions. Due to the highly sensitive nature of the surface scattering based signaling pathway from the ultrafine PtNWs, the ETS produces an accurate and sensitive signal at relative low concentrations of sulfate.

As shown in Figure 2a, distinguishable ETS characteristics were observed in the presence of a low concentration (μM level) of sulfate, indicating the efficiency of ETS for in situ characterization of the weak anionic surface adsorptions. Our results demonstrate that although it is considered a weakly adsorbed anion, sulfate can alter the surface adsorption process of a Pt based catalyst even at relatively low concentration. Specifically, while ETS signals do not show much difference at the hydrogen adsorption region, a slight decrease of ETS current with increasing sulfate concentrations was observed in a double layer region, indicating the surface adsorption of sulfate

DOI: 10.1021/acscentsci.8b00082
ACS Cent. Sci. 2018, 4, 590−599

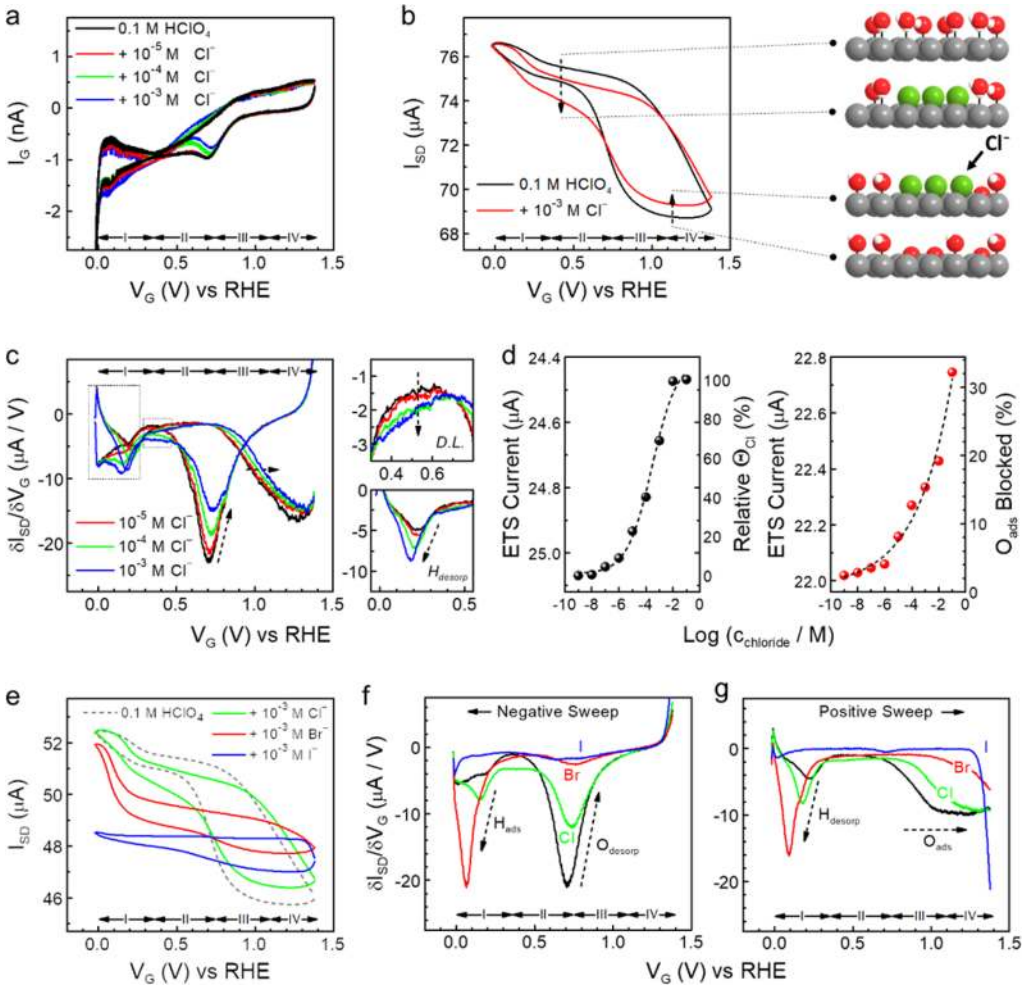

Figure 3. In situ ETS study of halide adsorption on Pt surface. (a) On-chip CV characteristics of a typical PtNW device in 0.1 M $HClO_4$ (black) and with addition of varying concentrations of sodium chloride. Redox regions of hydrogen adsorption (region I); the double layer (D.L.) (region II), reversible adsorption of OH (region III), and surface oxide formation (region IV) can be identified. (b) ETS characteristics of a typical PtNW device in 0.1 M $HClO_4$ (black) and with addition of 1 mM chloride anions (red). Dashed arrows indicate the change of ETS by the effect of chloride adsorption in double layer and oxidation regions, with corresponding illustrations of the surface adsorption models on the side. Pt atoms are gray, H atoms are white, O atoms are red, Cl atoms are green. (c) Differentiated ETS (dETS) results of PtNWs with varying chloride concentrations. Insets on the right depict the enlarged spectra at double layer and hydrogen desorption regions (dashed areas on the left). (d) ETS current of the PtNWs device in D.L. (left, value obtained at 0.5 V vs RHE) and oxidation (right, value obtained at 0.9 V vs RHE) regions at different chloride concentrations. Black dashed curves are sigmoidal (left) and exponential (right) fittings of the current values. Electrically derived surface coverage of Cl_{ads} at the D.L. region and percentage of blocked O_{ads} by Cl_{ads} in oxidation region are given at the corresponding right axis. (e) ETS characteristics of a typical PtNW device in 0.1 M $HClO_4$ (dashed black, as baseline comparison) and with addition of 1 mM chloride (green), bromide (red) and iodide (blue) anions. (f, g) dETS characteristics of halide adsorptions, results from negative (f) and positive (g) potential sweep are divided for the clarity of the comparison.

anions on the Pt surface, due to the stronger scattering of sulfate ions compared with surface adsorbed water molecules (Figure 2c). The most significant change in ETS signal is related to the adsorption of O species (Figure 2a, indicated by arrow 1), where there is a declining ETS current originated from Pt surface oxidation. As shown in Figure 2a, the ETS value of PtNWs is shifted to a higher value in the presence of sulfate ions, suggesting a smaller fraction of adsorbed oxygen species on the Pt surface. This result confirms that specific adsorption of sulfate anions occurs not only in the double layer region but also in the oxidation region, reducing the surface oxygen coverage in a large potential window. Since the surface coverage of oxygen species serves as an important intermediate step to many electrocatalytic energy conversion reactions (such as ORR),[1,2,30] surface information revealed by ETS characteristics is fundamentally important for the rational design and further optimization of electrocatalytic nanomaterials.

The differential analysis of ETS curve (dETS) (Figure 2b) leads to consistent conclusions: with increasing sulfate concentrations, the O_{ads} peak and the oxide reduction peak both show a decreasing trend in intensity (black dotted arrows 2 and 3 in Figure 2b). Additionally, an obvious shift can be easily identified in the OH_{ads} region (region III, as indicated by the red dotted arrow in Figure 2b) in the dETS results, while the oxide formation region at higher potential (>1.2 V vs RHE) stays unaltered. This observation indicates the competitive sulfate adsorption occurs through coadsorption with the hydroxyl group on the Pt surface, and no additional sulfate anions are further adsorbed during the oxide formation at higher potentials (>1.2 V vs RHE).

DOI: 10.1021/acscentsci.8b00082
ACS Cent. Sci. 2018, 4, 590−599

Halide Adsorption on PtNWs. Halides are commonly seen as strong binding and poisoning species that undermine the electrokinetics of Pt-catalyzed reactions. Due to their abundance in natural and industrial environments, a mechanistic study of the halide adsorption (especially in trace amounts) on Pt catalysts is of both fundamental and practical significance. Historically, due to the lack of intrinsic infrared spectroscopic features, in situ studies of halide adsorption on Pt surface relied heavily on X-ray based spectroscopy[20,31−33] and nonlinear optical method of SHG.[33,34] For these approaches, sensitivity is a general challenge. X-ray based technologies have relied on synchrotron source for increased signals, often implemented with ultrathin electrochemical cells for reduced beam attenuation, and the studies were only performed at relatively high chloride concentrations (10^{-3} M).[20,31−33,35−37]

We have acquired ETS characteristics of halide anionic adsorption on the PtNWs in halide containing electrolytes (Figure 3). Figures 3a shows typical I_G-V_G CV characteristics with chloride (Figure 3a), along with the ETS (Figure 3b) and differentiated ETS (Figure 3c) signals acquired simultaneously. Compared with sulfate adsorption, the ETS characteristics of the PtNWs are altered much more significantly by chloride adsorption, particularly considering that the concentration of chloride is about 3 orders of magnitude smaller (Figure 3) than sulfate (Figure 2). This result offers direct evidence revealing much stronger binding of Cl_{ads} and a much more altered surface chemistry of the PtNWs in the given potential window. In the D.L. region, a clear drop in current is observed (indicated by dashed arrow in region II, Figure 3b) due to the specific adsorption of Cl_{ads} at the inner Helmholtz plane (IHP), which exerts a stronger scattering effect than surface adsorbed H_2O molecules. In the O_{ads} region, a noticeable *increase* in the ETS signals (a smaller reduction of ETS current in region IV, see dashed arrow in Figure 3b) is observed. Given the decreasing conductance in this region is originated from surface oxidation, this result suggests that the competitive Cl^- adsorption blocks the adsorption of oxygen species, leading to a reduced O_{ads} scattering (stronger than Cl_{ads} scattering).

The characteristic ETS signals (for Cl_{ads}) can also be translated into dETS results with several corresponding features (Figure 3c). First, the dETS level in the D.L. region is elevated with increasing concentrations of Cl^-, corresponding to the increasing adsorption of Cl^- on the PtNW surface. Second, both O_{ads} and O_{desop} peaks show a clear decrease in intensities, corresponding to the blocking of adsorption sites for O_{ads} by competitive Cl_{ads}. Additionally, a clear shift in the onset potential of O_{ads} peak is observed in the dETS spectra (highlighted by the dashed arrow), indicating an added overpotential for the adsorption of O species due to the Cl_{ads} blocking, which provides direct in situ surface evidence that the strong anionic adsorption alters the electrokinetics of intermediate steps for electrocatalytic reactions (such as ORR), leading to a poisoning effect.

Compared to sulfate, the ETS response from chloride adsorption shows certain unique features, such as a larger ETS current drop in the D.L. region and an obvious shift in O_{ads} dETS peak (Figure 3b,c). These differences indicate distinct effects of chloride (than sulfate) on O_{ads}: (i) sulfate adsorbs weakly (and to a lesser extent) on PtNW surface at D.L. region and coadsorbs together with OH_{ads}, whereas (ii) chloride adsorbs more strongly at the D.L. region with a higher surface coverage and adds additional overpotential for hydroxyl adsorption when OH_{ads} needs to replace Cl_{ads} at the adsorption sites.

In the H_{upd} region, due to Cl_{ads} in the D.L. region lower down the current baseline, the hydrogen adsorption/desorption produces a larger change in ETS signals (i.e., elongated H_{ads}/H_{desorp} curves in region I in Figure 3b). The similar maximum ETS current at the end of H_{upd} potential indicates the complete removal of Cl_{ads} on H_{ads} covered Pt surface. It should be noted that no additional "step" in ETS or "new peak" in dETS was observed for Cl^- adsorption/desorption in the H_{upd} region, indicating a gradual replacement of Cl_{ads} by H_{ads} with the negative potential sweep and vice versa. We would also like to point out that the enlarged response in H_{upd} and a dropped current with a slightly increased slope in D.L. resembles the ETS characteristic of PtNWs in our previous report.[15] Our new results indicate that the previously established ETS characteristic of PtNWs was affected by trace amounts of Cl contaminations, which was probably due to electrolyte leakage from Ag/AgCl reference electrode.

The characteristic ETS response in the D.L. and O_{upd} region for chloride adsorption can be further utilized to obtain a direct (in situ) quantitative measure of the PtNW surface. Results shown in Figure 3d are obtained from a series of ETS signals at different chloride concentrations (see Supplementary Figure S3), at the potential of 0.5 V vs RHE (corresponding to the D.L. region) and 0.9 V vs RHE (corresponding to the O_{upd} region, which is indicative for the electrokinetics during ORR). Quantitative analysis of ETS currents show adsorption kinetics of chloride at specific potentials, with electrically determined surface coverage of Cl_{ads} (in D.L., Figure 3d left) and blockage of O_{ads} by Cl_{ads} (in O_{upd}, Figure 3d right). As shown in Figure 3d, Cl^- coverage significantly increases at the onset concentration of ∼1 μM in both regions. At high concentrations, Cl− adsorption shows a different behavior: while saturated coverage of Cl_{ads} was achieved at ∼10 mM at D.L., continuously increased blocking of the O_{ads} site is observed with increasing concentrations of Cl^- in the O_{upd} region. These results agree well with those derived from SHG (D.L.)[34] and electrochemical (O_{upd})[20,38] measurements, and demonstrate a quantitative approach that works for the entire potential window, with better sensitivity and accuracy for the characterizations of low concentration analyte in a much smaller sample volume.

We have further explored the adsorption characteristics of other halide anions, such as bromide and iodide, on the PtNW surface using the ETS approach. Figure 3e−g presents typical ETS and dETS characteristics of the PtNWs with chloride, bromide, and iodide adsorption (results are obtained from the same device to eliminate device variations). As evident from the results, Br_{ads} produces a qualitatively similar yet much stronger ETS signal on PtNWs to that of Cl_{ads}, with a more pronounced drop of ETS current in the D.L. region, an increase of ETS current in the oxide formation region, elongated ETS curves in the H_{upd} region, along with a corresponding H_{upd} peak increase/O_{ads} shift in dETS results. The qualitatively similar yet quantitatively stronger ETS signals from Br_{ads} are consistent with a stronger binding of Br_{ads} to Pt surface compared with Cl_{ads}. For Pt−I_{ads}, it is commonly known that an irreversibly adsorbed zerovalent iodine monolayer is formed on the Pt surface upon exposure to iodide anions,[20,34] which remains stable over a wide potential range and strongly inhibits the hydrogen and oxygen adsorption on the Pt surface. This unique I_{ads} characteristic results in a "flat" ETS and dETS curves, with

DOI: 10.1021/acscentsci.8b00082
ACS Cent. Sci. 2018, 4, 590−599

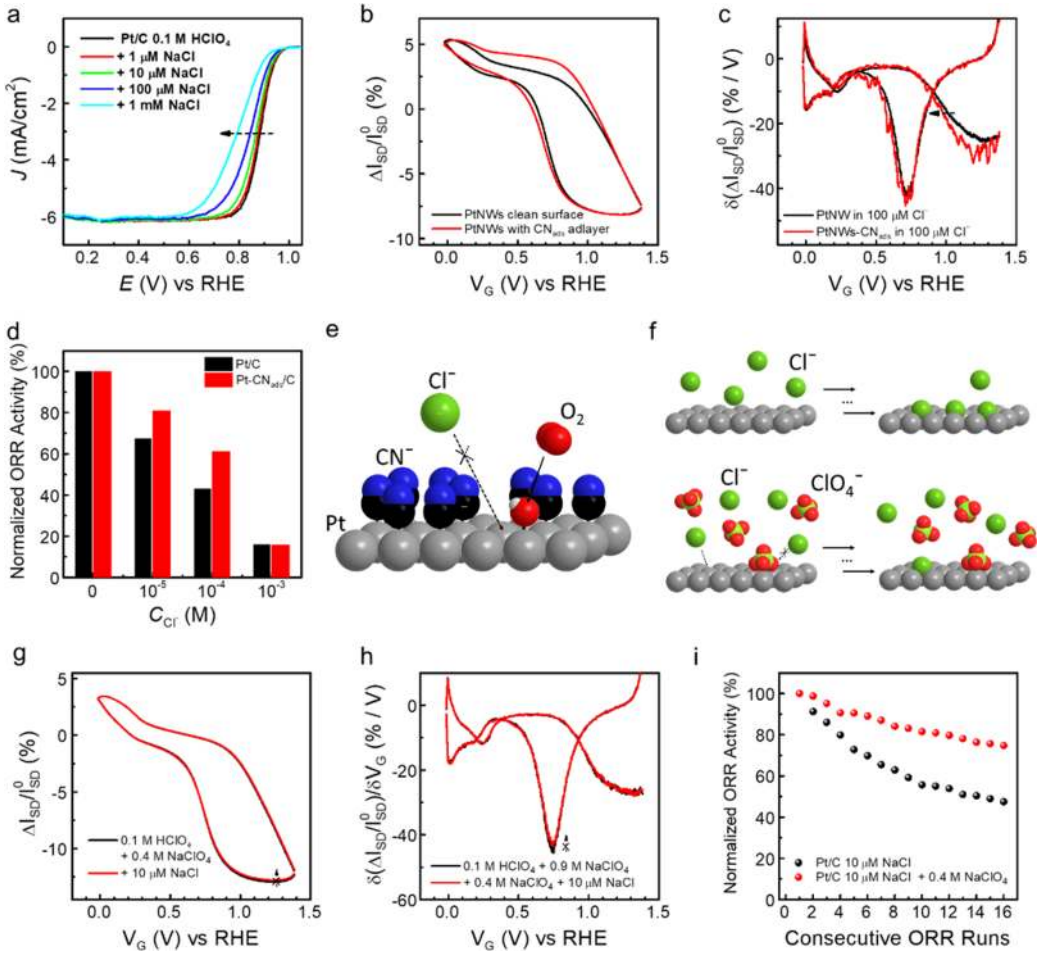

Figure 4. In situ ETS of competitive anionic adsorption and electrocatalytic performance of Pt-based catalysts. (a) Oxygen reduction reaction (ORR) polarization curves of commercial Pt/C on a rotating disk electrode (RDE) in $HClO_4$ (0.1 M) and with varying concentrations of Cl^-. (b) ETS characteristics of clean PtNW device (black) and PtNWs modified by a surface cyanide adlayer (red) in 0.1 M $HClO_4$. (c) Differentiated ETS (dETS) results of PtNWs (black) and cyanide modified PtNWs (PtNWs-CN_{ads}, red) in 0.1 M $HClO_4$ with 100 μM Cl^-. Dashed arrow indicates the recovery of Cl^- induced overpotential for O_{ads} peak after CN_{ads} modification. (d) Normalized ORR activities of clean (black) and CN_{ads} modified (red) Pt/C in response to different levels of Cl^- contaminations. (e) Proposed model for the enhanced Cl^- resistance through competitive surface adsorption. Cl^- adsorption is suppressed by a "static" CN_{ads} pattern, whereas adsorption of O species is unaffected. (f) Enhanced Cl^- resistance through "dynamic" competitive surface adsorption. Cl^- accumulation is suppressed by high concentration of perchlorate anions. Pt atoms are gray, H atoms are white, C atoms are black, N atoms are blue, O atoms are red, and Cl atoms are green. (g, h) ETS (g) and dETS (h) characteristics of Cl^- (10 μM) adsorptions on PtNWs in 0.1 M $HClO_4$ + 0.4 M $NaClO_4$. Dashed arrows show the lack of Cl_{ads} features in 0.4 M $NaClO_4$ containing electrolyte. (i) Evolution of ORR activities of Pt/C over consecutive runs (stability tests) in Cl^- (10 μM) contaminated electrolytes with or without high concentration (0.4 M) of $NaClO_4$.

only slight hydrogen and oxygen adsorption features at high overpotentials (Figure 3e,f).

The evolution of ETS characteristics for halide anions is consistent with their binding strength: $Cl^- < Br^- < I^-$, each with unique features that reveal the in situ surface processes in detail. Interestingly, the ETS signals of Cl_{ads} show a slight but obvious potential dependence in the D.L. region, i.e., a slightly increased slope in ETS and an elevated peak level in dETS (Figure 3b,c), whereas Br_{ads} and I_{ads} show a relative flat (potential independent) feature. These results indicate that in D.L. region, the surface adsorption (coverage) of Cl_{ads} gradually alters with the sweeping potential, whereas Br_{ads} and I_{ads} form a relatively stable layer that is potential independent. It should be noted that the potential dependence of halide adsorption in this specific region has received conflicting conclusions from different spectroscopic and electrochemical studies,[34] and our ETS investigation provides important experimental evidence and additional insights to resolve these controversies.

Anionic Competition on Pt Surface and Their Influence on ORR Performance. Chloride adsorption is further probed in competitive environments in order to establish its links to the electrokinetics of Pt catalyzed ORR. As demonstrated by ETS studies, the presence of sulfate or chloride anions (even at low concentrations) severely impedes the surface adsorption of O species, which may influence the overall ORR kinetics on Pt-based catalysts. Figure 4a depicts the polarization curves for Pt/C catalyzed ORR obtained in a rotating disk electrode (RDE) in clean and Cl^- contaminated electrolytes, respectively. The ORR activity of Pt/C indeed shows a significant decay with increasing concentrations of Cl^-. The increased overpotential in the presence of Cl^- is consistent with the site blocking of O_{ads} by Cl_{ads} observed in ETS studies (Figure 3). To address such chloride poisoning effect for Pt-catalyzed ORR performance, Cl^- inhibition is desired yet challenging, as chloride adsorption is much stronger on the Pt surface, and the influence of Cl_{ads} starts at a much lower

DOI: 10.1021/acscentsci.8b00082
ACS Cent. Sci. 2018, 4, 590−599

contamination level (~10^{-6} M), which impedes the implementation of general characterization methods for accurate, comprehensive, and practically relevant (trace concentration) studies. Importantly, the ability of ETS to provide highly sensitive, *in operando*, and surface specific characterization of Cl^- adsorption opens a highly efficient pathway to explore possible approaches to address this issue from a fundamental perspective. Using ETS as an effective probe, we demonstrate two types of anodic competition for Cl_{ads} on the Pt surface: a "static" anionic cyanide adlayer, and a "dynamic" high ionic strength electrolyte (high concentration of perchloric anions).

Cyanide (CN^-) adsorbs irreversibly on the Pt surface and forms a stable and relatively inert adlayer. Due to the unique molecular patterns of CN_{ads} on the Pt(111) surface, it has been successfully applied to provide fundamental insights into various electrocatalytic reactions.[39−41] We first employed ETS measurement to study the general surface adsorption characteristics of CN^- modified PtNW surface (PtNW-CN_{ads}). The overall conductivity of PtNWs shows a significant drop after the formation of a surface CN_{ads} adlayer, as expected from the additional CN_{ads} induced scattering (see Supplementary Figure S4). Interestingly, despite the absolute drop in current, the ETS characteristics of PtNW-CN_{ads} in $HClO_4$ remain largely unchanged (at H_{upd} and O_{upd} region) compared to that of PtNWs, as shown in Figure 4b (also see Supplementary Figure S4). We can therefore conclude that while CN_{ads} blocked the surface Pt atoms onto which they adsorb, the CN-free sites on the Pt surface are unaffected for the adsorption of H, H_2O, and O species. This characteristic is entirely different from that of other strong binding molecules such as bromide, iodide (Figure 3e,f), or CO.[15] Another noticeable difference in ETS is that PtNW-CN_{ads} demonstrate a more "flat" line in the D.L. region, indicating the blocked adsorption of tetrahedral anions (perchlorate with the weakest binding strength in this case) by the CN_{ads} patterning on the Pt surface. The above hypotheses have been previously proposed to explain the catalytic performance of cyanide modified Pt electrodes,[39,41] and the ETS characterization provides a direct (surface) and straightforward experimental support.

We further investigated the Cl^- adsorption on the PtNW-CN_{ads} surface using dETS characteristics of Cl^- adsorption on PtNW and PtNW-CN_{ads} surface (Figure 4c). The potential shift of O_{ads} peak induced by 100 μM Cl^- is partially reversed on the PtNW-CN_{ads} surface. This result indicates that the overpotential for OH adsorption (caused by Cl_{ads} blocking) on PtNW surfaces is reduced by the formation of a CN_{ads} adlayer (highlighted by the black arrows), *which inhibits the Cl^- adsorption presumably by electrostatic repulsion and/or steric hindering*. As the ORR activity of Pt surface is highly dependent on the electrokinetics of OH adsorption, such ETS results suggest that the resistance of Pt-based catalyst to Cl^- poisoning can be enhanced by CN_{ads} adlayer modification. We further tested this theory by evaluating the ORR activity of Pt/C in RDE measurements (Figure 4d). The unmodified Pt/C shows a significantly decreased current density in response to different levels of Cl^- contamination. After CN_{ads} modification, the relative current density drop became smaller, demonstrating enhanced resistance to Cl^- poisoning. The schematic model for such enhanced Cl^- resistance is summarized in Figure 4e. It should be noted that Pt/C−CN_{ads} show chloride resistance at low concentrations of 10 μM and 100 μM, but not at a high concentration of 1 mM. Interestingly, this quantitative trend is highly correlated to the ETS indicators, which show response in 10 μM and 100 μM of Cl^-, but not in 1 mM (see Supplementary Figure S5).

The Cl^- adsorption was further probed under a high concentration of perchloric anions (one of the weakest binding anions on Pt[20]), with the intention to understand how weakly adsorbed anions can affect the strongly adsorbed anions at extreme concentration difference. Figure 4g,h depicts the ETS and dETS results of PtNWs in the presence of Cl^- with high concentrations of ClO_4^- (0.4 M). Comparing the ETS and dETS data obtained in electrolyte with high concentration of ClO_4^- (0.4 M) with or without the presence of low level Cl^- (10 μM), it is apparent that the influence of Cl^- is negligible (no obvious O_{ads} overpotential, no current level change in the O_{upd} region, as indicated by dashed arrows in Figure 4g,h), in stark contrast to the test conducted in electrolyte with low concentration of ClO_4^- (0.1 M) (Figure 3b,c). This result suggests that dynamic competitive adsorption ClO_4^- in high concentration of ClO_4^- electrolyte can also increase Cl^- resistance, in a manner different from the "static" surface CN_{ads} adlayer. On the other hand, we note that ClO_4^- itself can reduce the ORR current (Supplementary Figure S6) and therefore is not an ideal way to optimize the fuel cell performance. Nonetheless, such anionic competitive behavior may offer other benefits. As shown in Figure 4i, for Pt-catalyzed ORR, not only does Cl^- contamination increase the overpotential and reduce the current density, it also shows an accumulating effect that continuously poisons the ORR performance over time. This accumulating effect could potentially cause serious activity degradation over time and thus a long-term durability problem to the real-world devices, such as polymer exchange membrane fuel cells (PEMFCs).[42,43] Importantly, in electrolyte with a high concentration of ClO_4^-, the current drop over consecutive tests in Cl^- containing electrolyte is greatly reduced. The reduced Cl_{ads} accumulation can be rationalized by competition from ClO_4^- anions, as indicated by the ETS results. Such behavior only occurs at 10 μM of Cl^-; concentrations higher than 100 μM Cl^- still show influence on the surface adsorption processes on Pt with the same ClO_4^- concentration, as confirmed by both RDE and ETS (see Supplementary Figure S6). Through our interfacial study, we have discovered a novel anion competition mechanism that significantly reduces the accumulation of halide adsorption on the Pt surface. It therefore offers a promising solution, by simply optimizing the electrolyte content, to increase the impurity tolerance of fuel cell devices and their long-term durability.

CONCLUSIONS

Together, with the direct experimental evidence derived from a unique nanoelectronic measurement, we have investigated the surface adsorption features of various anions (such as sulfate, halides, and cyanides) on the platinum catalyst, and demonstrated quantitatively that the competitive anionic adsorption can have a profound effect on ORR activity. The combination of electrochemical and nanoelectronic measurements produces highly sensitive and surface specific signals for exploring electrochemical interfaces with considerable precision and accuracy, allowing for the first time both qualitative and quantitative analysis at a low level of target analytes. It is especially efficient for the in situ characterization of surface adsorbed anions without distinct infrared spectroscopic features (such as halides), and those that do not generate specific electrochemical features (e.g., CV peaks). For similar reasons,

DOI: 10.1021/acscentsci.8b00082
ACS Cent. Sci. 2018, 4, 590−599

this on-chip approach is also appealing for the electrochemical interface that involves cations, which tailor the ORR activities via noncovalent interactions with surface oxygenated species[2,44−48] yet are difficult to study for their lack of spectroscopic feature. Related ETS studies of cationic impact are currently underway. The unique adsorption kinetics of each anion tested in this work and its influence on the corresponding oxygen species are used to rationalize the dependency of important Pt-catalyzed reactions (such as ORR) on anionic contamination. On the basis of the ETS descriptor for the ORR performance, we further investigated the chloride poisoning behavior in more complex anionic environments and demonstrate potential strategies to mitigate the poisoning effect using either a "static" anionic cyanide adlayer (that could hinder Cl^- adsorption and reduce the Cl_{ads} induced overpotential) or a "dynamic" high ionic strength approach (that helps prevent the long-term accumulation of Cl^- poisoning) for improved efficiency and stability of real-world energy conversion devices.

METHODS

Fabrication of the PtNWs Electrochemical Device. A PtNWs device was fabricated using a previously described approach.[15,23] Typically, a poly(methyl methacrylate) (PMMA, A8, MicroChem Corp.) film was prepared by spin-coating on the substrate (p++ silicon wafer with 300 nm thermal oxide) surface with prepatterned Au electrodes (Ti/Au, 50 nm/50 nm). E-beam lithography was then used to open windows on PMMA, which created desired patterns on the substrate. The preprepared (by cosolvent evaporation) free-standing film of PtNWs was then deposited onto the substrate surface. After the removal of PMMA template, PtNWs was deposited on the device substrate with desired patterns. To eliminate the influence of electrolyte and to avoid electrochemical reactions on the metal electrodes, another layer of PMMA (∼500 nm thick, electrochemically inert) was then deposited on the PtNWs device with spin-coating. A smaller window that only exposes PtNWs was opened by e-beam lithography. The final device, with exposed PtNWs and PMMA protected electrodes, was used for on-chip electrochemistry and in situ electrical spectroscopy.

Instead of an open chamber configuration,[15] a microfluidic setup was used in this work to achieve more efficient control of the electrolytes exposed to the PtNW device. A PDMS microfluidic channel was mounted on the Si chip with the channel aligned with the central region where the PtNW device is located. Polyethylene tubing was attached to the inlet and the outlet holes on the PDMS channel, and $HClO_4$ solutions or mixed electrolytes containing $HClO_4$ and desired anions (for introducing each anion, the corresponding sodium salt is used) were drawn through the channel using a syringe pump. The typical flow rate was 1 mL·h^{-1} during ETS tests and 10 mL·h^{-1} for the electrolyte switching. All electrolytes were degassed with ultrahigh purity nitrogen before use. For surface cyanide modification, the electrochemically cleaned PtNW devices were exposed to 0.1 M KCN solution for 30 min under open circuit, followed by extensive rinsing with the flow of DI water and then the 0.1 M $HClO_4$ electrolyte. No unexpected or unusually high safety hazards were encountered.

On-Chip CV and ETS Measurements. A two-channel source-measure unit (SMU, Keysight B2902a) was used for ETS measurements. A first SMU channel was used as a potentiostat to perform the on-chip CV by applying the potential (V_G) of source/drain electrode (acting as working electrode) as to the reference electrode (leak-free Ag/AgCl), while collecting the current (I_G) through the counter electrode (Pt wire). In a typical CV measurement, the scan rate is 28 mV s^{-1}. A second SMU channel was used to record ETS signals by supplying a small bias potential (50 mV) between source and drain electrodes and collecting the electrical conductive current (I_{SD}). See Supplementary Figure S2 for details.

For a typical measurement in this study, the gate (Faradaic) current is generally several orders of magnitude smaller than the ETS current ($I_G \approx 1$ nA and $I_{SD} \approx 50$ μA). Therefore, the on-chip CV current does not affect the ETS current, and no additional background subtraction or other mathematical treatment is needed before the data analysis. In case the electrochemical I_G is significant enough to affect the accuracy of I_{SD}, an equivalent circuit[16] can be used to subtract the I_G background from the ETS (I_{SD}) channel; see Supplementary Figure S7 for more detailed discussion.

Normalization of the I_{SD}−V_G Results. In an aqueous environment under open circuit, the conduction electrons were at least scattered by surface adsorbed water molecules, and the conductance of PtNWs at this stage is considered as a "baseline" conductive current (I_{SD}^0). This baseline value can be determined before each electrical spectroscopic scan by measuring the I−V characteristics of PtNWs with no V_G applied. With I_{SD}^0 measured, the I_{SD} of each test could also be normalized to relative conductance change ($\Delta I_{SD}/I_{SD}^0$). This normalization does not change the characteristic of each I_{SD}−V_G curve, and makes the comparison between different scans and different devices more reasonable, as the baseline conductance of each device are different and each could drift during measurements, due to the reasons such as Pt atom dissolution. The shape of I_{SD}, G_{SD}, and ΔG_{SD} are the same, and in the paper this characteristic is all referred as the ETS result. In the presence of strongly adsorbed anions such as halide, the "baseline" conductive current is also affected by the specially adsorbed anions under an open circuit. Note that in such case the "baseline" surface condition is changed from clean $HClO_4$ to that containing halide anions. Therefore, the comparison of absolute ETS current is more appropriate and more accurate in the study of halide adsorption and is thus adapted in this work.

ASSOCIATED CONTENT

Supporting Information

The Supporting Information is available free of charge on the ACS Publications website at DOI: 10.1021/acscentsci.8b00082.

Additional experimental methods, characterizations, results, and discussion (PDF)

AUTHOR INFORMATION

Corresponding Authors

*(Y.H.) E-mail: yhuang@seas.ucla.edu.

*(X.D.) E-mail: xduan@chem.ucla.edu.

ORCID

Mengning Ding: 0000-0001-6581-3385

Yu Huang: 0000-0003-1793-0741

Xiangfeng Duan: 0000-0002-4321-6288

Present Address

#(M.D.) Key Laboratory of Mesoscopic Chemistry, School of Chemistry and Chemical Engineering, Nanjing University, Nanjing 210023, China

DOI: 10.1021/acscentsci.8b00082
ACS Cent. Sci. 2018, 4, 590−599

Author Contributions

M.D., X.D. and Y.H. designed the research; M.D., G.Z., Z.Z., Z.H., M.L., Y.L., and H.-Y.S. performed the research, M.D., X.D., and Y.H. analyzed the data, and M.D., X.D., and Y.H. wrote the paper.

Notes

The authors declare no competing financial interest.

■ ACKNOWLEDGMENTS

We acknowledge the support by the NSF Award 1508692.

■ REFERENCES

(1) Seh, Z. W.; Kibsgaard, J.; Dickens, C. F.; Chorkendorff, I.; Nørskov, J. K.; Jaramillo, T. F. Combining theory and experiment in electrocatalysis: Insights into materials design. *Science* **2017**, *355*, eaad4998.

(2) Stamenkovic, V. R.; Strmcnik, D.; Lopes, P. P.; Markovic, N. M. Energy and fuels from electrochemical interfaces. *Nat. Mater.* **2017**, *16*, 57−69.

(3) Montoya, J. H.; Seitz, L. C.; Chakthranont, P.; Vojvodic, A.; Jaramillo, T. F.; Norskov, J. K. Materials for solar fuels and chemicals. *Nat. Mater.* **2017**, *16*, 70−81.

(4) Roger, I.; Shipman, M. A.; Symes, M. D. Earth-abundant catalysts for electrochemical and photoelectrochemical water splitting. *Nat. Rev. Chem.* **2017**, *1*, 0003.

(5) Mistry, H.; Varela, A. S.; Kühl, S.; Strasser, P.; Cuenya, B. R. Nanostructured electrocatalysts with tunable activity and selectivity. *Nat. Rev. Mater.* **2016**, *1*, 16009.

(6) Wang, C.; Markovic, N. M.; Stamenkovic, V. R. Advanced Platinum Alloy Electrocatalysts for the Oxygen Reduction Reaction. *ACS Catal.* **2012**, *2*, 891−898.

(7) Wu, J.; Yang, H. Platinum-Based Oxygen Reduction Electrocatalysts. *Acc. Chem. Res.* **2013**, *46*, 1848−1857.

(8) Bu, L.; Zhang, N.; Guo, S.; Zhang, X.; Li, J.; Yao, J.; Wu, T.; Lu, G.; Ma, J.-Y.; Su, D.; Huang, X. Biaxially strained PtPb/Pt core/shell nanoplate boosts oxygen reduction catalysis. *Science* **2016**, *354*, 1410−1414.

(9) Li, M.; Zhao, Z.; Cheng, T.; Fortunelli, A.; Chen, C.-Y.; Yu, R.; Zhang, Q.; Gu, L.; Merinov, B.; Lin, Z.; Zhu, E.; Yu, T.; Jia, Q.; Guo, J.; Zhang, L.; Goddard, W. A.; Huang, Y.; Duan, X. Ultrafine jagged platinum nanowires enable ultrahigh mass activity for the oxygen reduction reaction. *Science* **2016**, *354*, 1414−1419.

(10) Escudero-Escribano, M.; Malacrida, P.; Hansen, M. H.; Vej-Hansen, U. G.; Velázquez-Palenzuela, A.; Tripkovic, V.; Schiøtz, J.; Rossmeisl, J.; Stephens, I. E. L.; Chorkendorff, I. Tuning the activity of Pt alloy electrocatalysts by means of the lanthanide contraction. *Science* **2016**, *352*, 73−76.

(11) Huang, X.; Zhao, Z.; Cao, L.; Chen, Y.; Zhu, E.; Lin, Z.; Li, M.; Yan, A.; Zettl, A.; Wang, Y. M.; Duan, X.; Mueller, T.; Huang, Y. High-performance transition metal−doped Pt_3Ni octahedra for oxygen reduction reaction. *Science* **2015**, *348*, 1230−1234.

(12) Zhang, L.; Roling, L. T.; Wang, X.; Vara, M.; Chi, M.; Liu, J.; Choi, S.-I.; Park, J.; Herron, J. A.; Xie, Z.; Mavrikakis, M.; Xia, Y. Platinum-based nanocages with subnanometer-thick walls and well-defined, controllable facets. *Science* **2015**, *349*, 412−416.

(13) Chen, C.; Kang, Y.; Huo, Z.; Zhu, Z.; Huang, W.; Xin, H. L.; Snyder, J. D.; Li, D.; Herron, J. A.; Mavrikakis, M.; Chi, M.; More, K. L.; Li, Y.; Markovic, N. M.; Somorjai, G. A.; Yang, P.; Stamenkovic, V. R. Highly Crystalline Multimetallic Nanoframes with Three-Dimensional Electrocatalytic Surfaces. *Science* **2014**, *343*, 1339−1343.

(14) Stephens, I. E. L.; Rossmeisl, J.; Chorkendorff, I. Toward sustainable fuel cells. *Science* **2016**, *354*, 1378−1379.

(15) Ding, M.; He, Q.; Wang, G.; Cheng, H.-C.; Huang, Y.; Duan, X. An on-chip electrical transport spectroscopy approach for in situ monitoring electrochemical interfaces. *Nat. Commun.* **2015**, *6*, 7867.

(16) Ding, M.; et al. Nanoelectronic Investigation Reveals the Electrochemical Basis of Electrical Conductivity in *Shewanella* and. *ACS Nano* **2016**, *10*, 9919−9926.

(17) Voiry, D.; et al. The role of electronic coupling between substrate and 2D MoS_2 nanosheets in electrocatalytic production of hydrogen. *Nat. Mater.* **2016**, *15*, 1003−1009.

(18) Wang, P.; Yan, M.; Meng, J.; Jiang, G.; Qu, L.; Pan, X.; Liu, J. Z.; Mai, L. Oxygen evolution reaction dynamics monitored by an individual nanosheet-based electronic circuit. *Nat. Commun.* **2017**, *8*, 645.

(19) Zhang, J.; et al. Unveiling Active Sites for the Hydrogen Evolution Reaction on Monolayer MoS2. *Adv. Mater.* **2017**, *29*, 1701955.

(20) Marković, N. M.; Ross, P. N., Jr. Surface science studies of model fuel cell electrocatalysts. *Surf. Sci. Rep.* **2002**, *45*, 117−229.

(21) Xia, B. Y.; Wu, H. B.; Yan, Y.; Lou, X. W.; Wang, X. Ultrathin and Ultralong Single-Crystal Platinum Nanowire Assemblies with Highly Stable Electrocatalytic Activity. *J. Am. Chem. Soc.* **2013**, *135*, 9480−9485.

(22) Climent, V.; Feliu, J. Thirty years of platinum single crystal electrochemistry. *J. Solid State Electrochem.* **2011**, *15*, 1297−1315.

(23) Ding, M.; Liu, Y.; Wang, G.; Zhao, Z.; Yin, A.; He, Q.; Huang, Y.; Duan, X. Highly Sensitive Chemical Detection with Tunable Sensitivity and Selectivity from Ultrathin Platinum Nanowires. *Small* **2017**, *13*, 1602969.

(24) Yang, F.; Donavan, K. C.; Kung, S.-C.; Penner, R. M. The Surface Scattering-Based Detection of Hydrogen in Air Using a Platinum Nanowire. *Nano Lett.* **2012**, *12*, 2924−2930.

(25) Su, Z.; Climent, V.; Leitch, J.; Zamlynny, V.; Feliu, J. M.; Lipkowski, J. Quantitative SNIFTIRS studies of (bi)sulfate adsorption at the Pt(111) electrode surface. *Phys. Chem. Chem. Phys.* **2010**, *12*, 15231−15239.

(26) Zeng, D.-M.; Jiang, Y.-X.; Zhou, Z.-Y.; Su, Z.-F.; Sun, S.-G. In situ FTIR spectroscopic studies of (bi)sulfate adsorption on electrodes of Pt nanoparticles supported on different substrates. *Electrochim. Acta* **2010**, *55*, 2065−2072.

(27) Braunschweig, B.; Mukherjee, P.; Dlott, D. D.; Wieckowski, A. Real-Time Investigations of Pt(111) Surface Transformations in Sulfuric Acid Solutions. *J. Am. Chem. Soc.* **2010**, *132*, 14036−14038.

(28) Campbell, D. J.; Corn, R. M. Second harmonic generation studies of polycrystalline platinum electrodes in sulfuric and perchloric acid solutions. *J. Phys. Chem.* **1988**, *92*, 5796−5800.

(29) Fromondi, I.; Scherson, D. (Bi)Sulfate Adsorption on Quasiperfect Pt(111) Facets from Acidic Aqueous Electrolytes as Monitored by Optical Techniques. *J. Phys. Chem. C* **2007**, *111*, 10154−10157.

(30) Wang, C.; Li, D.; Chi, M.; Pearson, J.; Rankin, R. B.; Greeley, J.; Duan, Z.; Wang, G.; van der Vliet, D.; More, K. L.; Markovic, N. M.; Stamenkovic, V. R. Rational Development of Ternary Alloy Electrocatalysts. *J. Phys. Chem. Lett.* **2012**, *3*, 1668−1673.

(31) Arruda, T. M.; Shyam, B.; Ziegelbauer, J. M.; Mukerjee, S.; Ramaker, D. E. Investigation into the Competitive and Site-Specific Nature of Anion Adsorption on Pt Using In Situ X-ray Absorption Spectroscopy. *J. Phys. Chem. C* **2008**, *112*, 18087−18097.

(32) Russell, A. E.; Rose, A. X-ray Absorption Spectroscopy of Low Temperature Fuel Cell Catalysts. *Chem. Rev.* **2004**, *104*, 4613−4636.

(33) Magnussen, O. M. Ordered Anion Adlayers on Metal Electrode Surfaces. *Chem. Rev.* **2002**, *102*, 679−726.

(34) Campbell, D. J.; Lynch, M. L.; Corn, R. M. Second harmonic generation studies of anionic chemisorption at polycrystalline platinum electrodes. *Langmuir* **1990**, *6*, 1656−1664.

(35) Casalongue, H. S.; Kaya, S.; Viswanathan, V.; Miller, D. J.; Friebel, D.; Hansen, H. A.; Nørskov, J. K.; Nilsson, A.; Ogasawara, H. Direct observation of the oxygenated species during oxygen reduction on a platinum fuel cell cathode. *Nat. Commun.* **2013**, *4*, 2817.

(36) Sasaki, K.; Marinkovic, N.; Isaacs, H. S.; Adzic, R. R. Synchrotron-Based *In Situ* Characterization of Carbon-Supported Platinum and Platinum Monolayer Electrocatalysts. *ACS Catal.* **2016**, *6*, 69−76.

DOI: 10.1021/acscentsci.8b00082
ACS Cent. Sci. 2018, 4, 590−599

(37) Liu, X.; Yang, W.; Liu, Z. Recent Progress on Synchrotron-Based In-Situ Soft X-ray Spectroscopy for Energy Materials. *Adv. Mater.* **2014**, *26*, 7710−7729.
(38) Novak, D. M.; Conway, B. E. Competitive adsorption and state of charge of halide ions in monolayer oxide film growth processes at Pt anodes. *J. Chem. Soc., Faraday Trans. 1* **1981**, *77*, 2341−2359.
(39) Ciapina, E. G.; Lopes, P. P.; Subbaraman, R.; Ticianelli, E. A.; Stamenkovic, V.; Strmcnik, D.; Markovic, N. M. Surface spectators and their role in relationships between activity and selectivity of the oxygen reduction reaction in acid environments. *Electrochem. Commun.* **2015**, *60*, 30−33.
(40) Cuesta, A. At Least Three Contiguous Atoms Are Necessary for CO Formation during Methanol Electrooxidation on Platinum. *J. Am. Chem. Soc.* **2006**, *128*, 13332−13333.
(41) Strmcnik, D.; Escudero-Escribano, M.; Kodama, K.; Stamenkovic, V. R.; Cuesta, A.; Marković, N. M. Enhanced electrocatalysis of the oxygen reduction reaction based on patterning of platinum surfaces with cyanide. *Nat. Chem.* **2010**, *2*, 880−885.
(42) Wu, J.; Yuan, X. Z.; Martin, J. J.; Wang, H.; Zhang, J.; Shen, J.; Wu, S.; Merida, W. A review of PEM fuel cell durability: Degradation mechanisms and mitigation strategies. *J. Power Sources* **2008**, *184*, 104−119.
(43) Ehteshami, S. M. M.; Taheri, A.; Chan, S. H. A review on ions induced contamination of polymer electrolyte membrane fuel cells, poisoning mechanisms and mitigation approaches. *J. Ind. Eng. Chem.* **2016**, *34*, 1−8.
(44) Dunwell, M.; Wang, J.; Yan, Y.; Xu, B. Surface enhanced spectroscopic investigations of adsorption of cations on electrochemical interfaces. *Phys. Chem. Chem. Phys.* **2017**, *19*, 971−975.
(45) Chen, X.; McCrum, I. T.; Schwarz, K. A.; Janik, M. J.; Koper, M. T. M. Co-adsorption of Cations as the Cause of the Apparent pH Dependence of Hydrogen Adsorption on a Stepped Platinum Single-Crystal Electrode. *Angew. Chem., Int. Ed.* **2017**, *56*, 15025−15029.
(46) Berkes, B. B.; Inzelt, G.; Schuhmann, W.; Bondarenko, A. S. Influence of Cs^+ and Na^+ on Specific Adsorption of *OH, *O, and *H at Platinum in Acidic Sulfuric Media. *J. Phys. Chem. C* **2012**, *116*, 10995−11003.
(47) Strmcnik, D.; van der Vliet, D. F.; Chang, K. C.; Komanicky, V.; Kodama, K.; You, H.; Stamenkovic, V. R.; Marković, N. M. Effects of Li^+, K^+, and Ba^{2+} Cations on the ORR at Model and High Surface Area Pt and Au Surfaces in Alkaline Solutions. *J. Phys. Chem. Lett.* **2011**, *2*, 2733−2736.
(48) Strmcnik, D.; Kodama, K.; van der Vliet, D.; Greeley, J.; Stamenkovic, V. R.; Marković, N. M. The role of non-covalent interactions in electrocatalytic fuel-cell reactions on platinum. *Nat. Chem.* **2009**, *1*, 466−472.

DOI: 10.1021/acscentsci.8b00082
ACS Cent. Sci. 2018, 4, 590−599